A FINITE ELEMENT METHOD FOR CLASSICAL PLATE THEORY

by Stephen V. Harren
http://www.harren.us

0. Table of Contents

1. Governing Equations

Here the governing equations of classical plate theory in Cartesian coordinates are listed. Some of the equations below contain the two-dimensional alternating symbol

$$\varepsilon_{ij} = \begin{bmatrix} 0 & 1 \\ -1 & 0 \end{bmatrix}, \tag{1.1}$$

which possesses the properties $\varepsilon_{ij} = -\varepsilon_{ji}$, $\varepsilon_{ij}\varepsilon_{jk} = -\delta_{ik}$, and $\varepsilon_{ji}\varepsilon_{jk} = \delta_{ik}$, where δ_{ik} are the components of the two-dimensional identity matrix (the so-called Kronecker delta).

Denoting u as the transverse displacement of the plate, the rotation vector ϕ_i and the curvature tensor κ_{ij} are

$$\phi_i = \varepsilon_{ij} u_{,j} \ , \qquad \kappa_{ij} = u_{,ij} \ , \tag{1.2}$$

where the comma represents differentiation with respect to the spatial coordinates. Hooke's Law is

$$\begin{aligned} M_{xx} &= -M_{yy} = \frac{Eh^3}{12(1+\nu)}\, \kappa_{xy} \, , \\ M_{xy} &= -\frac{Eh^3}{12(1-\nu^2)} \left[\kappa_{xx} + \nu \kappa_{yy} \right] , \\ M_{yx} &= \frac{Eh^3}{12(1-\nu^2)} \left[\nu \kappa_{xx} + \kappa_{yy} \right] . \end{aligned} \tag{1.3}$$

In eqns. (1.3), E is Young's modulus, ν is Poisson's ratio, M_{ij} are the components of the moment tensor, and h is the plate thickness. Note that M_{ij} is the moment vector in the j–direction acting on the face whose normal is the i–direction. Notwithstanding, eqns. (1.3) can be written in tensorial form as

$$\begin{aligned} M_{im}\varepsilon_{mj} &= (\mathbf{M} \cdot \boldsymbol{\varepsilon})_{ij} = C_{ijkl}\kappa_{lk} \, , \\ C_{ijkl} &= \frac{Eh^3}{12(1-\nu^2)} \left[(1-\nu) I_{ijkl} + \nu \delta_{ij}\delta_{kl} \right] , \qquad I_{ijkl} = \frac{1}{2}\left(\delta_{ik}\delta_{jl} + \delta_{jk}\delta_{il} \right) . \end{aligned} \tag{1.4}$$

Now, moment equilibrium is

$$M_{ji,j} + \varepsilon_{ij} V_j = 0 \quad \text{or} \quad M_{ji,j}\varepsilon_{ik} + V_k = 0 \ , \tag{1.5}$$

which when written out, is

$$V_x = M_{xy,x} + M_{yy,y} \quad \text{and} \quad V_y = -M_{xx,x} - M_{yx,y} \, , \tag{1.6}$$

where V_i are the components of the internal shear vector. Next, transverse equilibrium is

$$V_{i,i} + q = 0 \, , \tag{1.7}$$

where q is the distributed load (force per unit area acting in the z–direction).

Finally, substitution of eqns. (1.3) into eqns. (1.6) gives Hooke's Law for the shear vector

$$V_i = -\frac{Eh^3}{12(1-\nu^2)} \left(\nabla^2 u \right)_{,i} \ , \tag{1.8}$$

where $\nabla^2 u = u_{,xx} + u_{,yy}$ is the Laplacian of u, and which when put into eqn. (1.7) yields the governing equation of the plate, *viz.,*

$$\frac{Eh^3}{12(1-\nu^2)} \nabla^4 u = q \, . \tag{1.9}$$

In eqn. (1.9), $\nabla^4 u = u_{,xxxx} + 2u_{,xxyy} + u_{,yyyy}$ is the bi-harmonic of u.

Turning attention to polar coordinates, eqns. (1.2) are

$$\phi_r = \frac{1}{r}\,u_{,\theta}\ , \qquad \phi_\theta = -u_{,r}\ ,$$
$$\kappa_{rr} = u_{,rr}\ , \qquad \kappa_{\theta\theta} = \frac{1}{r^2}\,u_{,\theta\theta} + \frac{1}{r}u_{,r}\ , \qquad \kappa_{r\theta} = \kappa_{\theta r} = \frac{1}{r}u_{,r\theta} - \frac{1}{r^2}u_{,\theta}\ . \tag{1.10}$$

In polar coordinates, Hooke's Law (1.3) is obtained by making the replacements $x \to r$ and $y \to \theta$
Now, eqns. (1.8) become in polar coordinates

$$V_r = -\frac{Eh^3}{12(1-\nu^2)}\left[\,u_{,rrr} + \frac{1}{r}\,u_{,rr} - \frac{1}{r^2}u_{,r} + \frac{1}{r^2}u_{,r\theta\theta} - \frac{2}{r^3}u_{,\theta\theta}\,\right],$$
$$V_\theta = -\frac{Eh^3}{12(1-\nu^2)}\left[\,\frac{1}{r}u_{,rr\theta} + \frac{1}{r^2}u_{,r\theta} + \frac{1}{r^3}u_{,\theta\theta\theta}\,\right]. \tag{1.11}$$

Finally, the bi-harmonic operator in eqn. (1.9) is

$$\nabla^4 u = u_{,rrrr} + \frac{2}{r}u_{,rrr} - \frac{1}{r^2}u_{,rr} + \frac{2}{r^2}u_{,rr\theta\theta} + \frac{1}{r^3}u_{,r} - \frac{2}{r^3}u_{,r\theta\theta} + \frac{4}{r^4}u_{,\theta\theta} + \frac{1}{r^4}u_{,\theta\theta\theta\theta}\ . \tag{1.12}$$

2. The Principle of Virtual Work

Let u^* be an arbitrary, twice differentiable function (the so-called virtual displacement). By the product rule of differentiation then, $(u^*V_i)_{,i} = u^*_{,i}V_i + u^*V_{i,i}$. Substitute the transverse equilibrium eqn. (1.7) into this result to obtain

$$u^*_{,i}V_i = (u^*V_i)_{,i} + u^*q\ . \tag{2.1}$$

Now, the virtual rotation vector is $\phi^*_j = \varepsilon_{ji}u^*_{,i}$, and via the moment equilibrium equation (1.5) $V_i = -M_{kj,k}\varepsilon_{ji}$. Using these two results in eqn. (2.1) gives

$$-\phi^*_j M_{kj,k} = (u^*V_i)_{,i} + u^*q\ . \tag{2.2}$$

By the product rule of differentiation again $\left(\phi^*_j M_{kj}\right)_{,k} = \phi^*_{j,k}M_{kj} + \phi^*_j M_{kj,k}$. This result, when put into eqn. (2.2), yields

$$\phi^*_{j,i}M_{ij} = \left(\phi^*_j M_{ij}\right)_{,i} + (u^*V_i)_{,i} + u^*q\ . \tag{2.3}$$

Now, using Hooke's Law (1.4) and the definition of the virtual rotation vector, $\phi^*_{j,i}M_{ij} = u^*_{,ji}(\mathbf{M}\cdot\boldsymbol{\varepsilon})_{ij} = $
$= u^*_{,ji}C_{ijkl}u_{,lk}$, which, when put into eqn. (2.3), gives

$$u^*_{,ji}C_{ijkl}u_{,lk} = \left(\phi^*_j M_{ij}\right)_{,i} + (u^*V_i)_{,i} + u^*q\ . \tag{2.4}$$

Integrate eqn. (2.4) over the domain of the plate A, and use the Divergence Theorem to see

$$\int_A u^*_{,ji}C_{ijkl}u_{,lk}\ \mathrm{d}A = \oint_t \phi^*_j\mathcal{M}_j\ \mathrm{d}t + \oint_t u^*V_n\ \mathrm{d}t + \int_A u^*q\ \mathrm{d}A\ , \tag{2.5}$$

where $\mathcal{M}_j = n_iM_{ij}$ is the boundary moment vector and $V_n = n_iV_i$ is the normal component of the shear vector ($\mathbf{n}$ is the outward pointing unit normal vector on the boundary). Also, t is the circumferential coordinate around the boundary of the plate (measured in the counterclockwise sense).

While eqn. (2.5) is valid, the circuit integral terms need to be modified to agree with the admissible boundary equations of plate theory. Consequently, using $u^*_{,t} = \phi^*_n$, the product rule of differentiation gives $(u^*\mathcal{M}_n)_{,t} = \phi^*_n\mathcal{M}_n + u^*\mathcal{M}_{n,t}$. Integrating this around the circuit yields

$$\oint_t (u^* \mathcal{M}_n)_{,t} \, \mathrm{d}t = \oint_t \mathrm{d}(u^* \mathcal{M}_n) = 0 = \oint_t \phi_n^* \mathcal{M}_n \, \mathrm{d}t + \oint_t u^* \mathcal{M}_{n,t} \, \mathrm{d}t \tag{2.6}$$

or

$$\oint_t \phi_n^* \mathcal{M}_n \, \mathrm{d}t = - \oint_t u^* \mathcal{M}_{n,t} \, \mathrm{d}t \, . \tag{2.7}$$

Thus, via eqn. (2.7)

$$\oint_t \phi_j^* \mathcal{M}_j \, \mathrm{d}t + \oint_t u^* V_n \, \mathrm{d}t = \oint_t \phi_n^* \mathcal{M}_n \, \mathrm{d}t + \oint_t \phi_t^* \mathcal{M}_t \, \mathrm{d}t + \oint_t u^* V_n \, \mathrm{d}t = \oint_t \phi_t^* \mathcal{M}_t \, \mathrm{d}t + \oint_t u^* \bar{V}_n \, \mathrm{d}t \ , \tag{2.8}$$

where $\bar{V}_n = V_n - \mathcal{M}_{n,t}$ is the Kirchhoff shear force. Finally, then, substitution of eqn. (2.8) into eqn. (2.5) gives the Principle of Virtual Work, *viz.,*

$$\int_A u^*_{,ji} C_{ijkl} u_{,lk} \, \mathrm{d}A = \oint_t \phi_t^* \mathcal{M}_t \, \mathrm{d}t + \oint_t u^* \bar{V}_n \, \mathrm{d}t + \int_A u^* q \, \mathrm{d}A \ . \tag{2.9}$$

From eqn. (2.9), one sees that admissible boundary conditions for plate theory are: prescribe either ϕ_t or $\mathcal{M}_t$ on the boundary; and prescribe either u or $\bar{V}_n$.

3. Example in Cartesian Coordinates

Here, the solution to a simple problem in Cartesian coordinates is presented, which problem will be solved numerically later in **§8** with the finite element method.

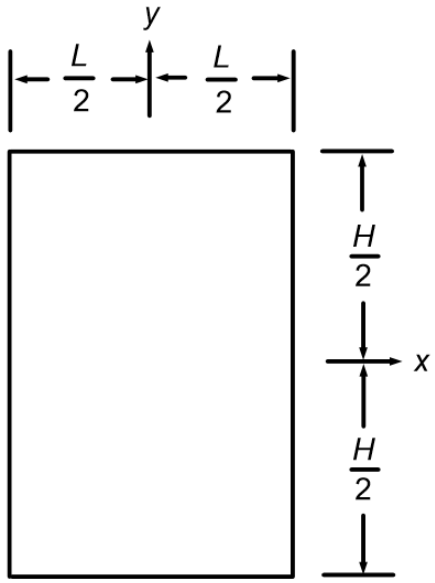

Figure 1. Domain of an L by H rectangular plate.

The domain of the rectangular plate under consideration is shown at left in Fig. 1. The plate is subject to the distributed load

$$q = -\frac{\pi^2 F}{4LH} \cos\left(\frac{\pi x}{L}\right) \cos\left(\frac{\pi y}{H}\right) , \tag{3.1}$$

where $F > 0$ is the net downward force of the distribution, *i.e.,*

$$\int_A q \mathrm{d}A = -F \, . \tag{3.2}$$

Note that q is zero on the boundary and is maximum at the origin. Hence the term "bubble." On all four faces the boundary conditions are

$$u = 0 \, , \qquad \mathcal{M}_t = 0 \, , \tag{3.3}$$

which are the so-called "simply-supported" boundary conditions.

The governing eqn. (1.9) is, via eqn. (3.1),

$$u_{,xxxx} + 2u_{,xxyy} + u_{,yyyy} = -\frac{3\pi^2 (1-\nu^2) F}{E h^3 LH} \cos\left(\frac{\pi x}{L}\right) \cos\left(\frac{\pi y}{H}\right) , \tag{3.4}$$

which is solved with a displacement of the form

$$u = k\cos\left(\frac{\pi x}{L}\right)\cos\left(\frac{\pi y}{H}\right). \tag{3.5}$$

Substituting eqn. (3.5) into eqn. (3.4) gives that

$$k = -\frac{3(1-\nu^2)}{\pi^2 E h^3}\left[\frac{L^3H^3}{(L^2+H^2)^2}\right]F. \tag{3.6}$$

With eqns. (3.5) and (3.6) the problem is solved.

By differentiation of eqn. (3.5) by way of the first eqns. (1.2), the rotation vector is

$$\phi_x = \frac{3(1-\nu^2)}{\pi^2 E h^3}\left[\frac{L^3H^2}{(L^2+H^2)^2}\right]F\cos\left(\frac{\pi x}{L}\right)\sin\left(\frac{\pi y}{H}\right),$$

$$\phi_y = -\frac{3(1-\nu^2)}{\pi^2 E h^3}\left[\frac{L^2H^3}{(L^2+H^2)^2}\right]F\sin\left(\frac{\pi x}{L}\right)\cos\left(\frac{\pi y}{H}\right). \tag{3.7}$$

Now, using the second of eqns. (1.2) and eqn. (1.3), the moment components are

$$M_{xx} = -M_{yy} = -\frac{(1-\nu)F}{4}\left[\frac{L^2H^2}{(L^2+H^2)^2}\right]\sin\left(\frac{\pi x}{L}\right)\sin\left(\frac{\pi y}{H}\right),$$

$$M_{xy} = -\frac{F}{4}\left[\frac{LH(\nu L^2+H^2)}{(L^2+H^2)^2}\right]\cos\left(\frac{\pi x}{L}\right)\cos\left(\frac{\pi y}{H}\right), \tag{3.8}$$

$$M_{yx} = \frac{F}{4}\left[\frac{LH(L^2+\nu H^2)}{(L^2+H^2)^2}\right]\cos\left(\frac{\pi x}{L}\right)\cos\left(\frac{\pi y}{H}\right).$$

Finally, differentiating eqns. (3.5) and using eqns. (1.8), one obtains the components of the shear vector

$$V_x = \frac{\pi F}{4}\left[\frac{H}{L^2+H^2}\right]\sin\left(\frac{\pi x}{L}\right)\cos\left(\frac{\pi y}{H}\right), \qquad V_y = \frac{\pi F}{4}\left[\frac{L}{L^2+H^2}\right]\cos\left(\frac{\pi x}{L}\right)\sin\left(\frac{\pi y}{H}\right). \tag{3.9}$$

Note that both the displacement u and the bending moments M_{xy} and M_{yx} are zero on the boundary so that the boundary conditions (3.3) are satisfied.

Now, at the upper right corner of the domain, the normal moment vector $\mathcal{M}_n^- = M_{xx}$ before the corner and $\mathcal{M}_n^+ = M_{yy}$ after the corner are, via the first of eqns. (3.8),

$$\mathcal{M}_n^- = -\mathcal{M}_n^+ = -\frac{(1-\nu)F}{4}\left[\frac{L^2H^2}{(L^2+H^2)^2}\right] \tag{3.10}$$

so that the corner force (at the upper right corner) is

$$\mathcal{M}_n^- - \mathcal{M}_n^+ = -\frac{(1-\nu)F}{2}\left[\frac{L^2H^2}{(L^2+H^2)^2}\right]. \tag{3.11}$$

4. Example in Polar Coordinates

Here a problem in polar coordinates is solved, which problem later will be solved numerically in **§9** with the finite element method. Specifically, below in Fig. 2 is shown the domain of a quarter-annular plate. The distributed load q is zero. The boundaries at $\theta = 0$ and $\theta = \pi/2$ are simply supported, *i.e.*,

$$u = 0\,, \qquad \mathcal{M}_t = 0\,, \tag{4.1}$$

while the inner radius $r = a$ is built in, *i.e.*,

$$u = \phi_t = 0\,. \tag{4.2}$$

A transverse sinusoidal edge traction is applied to the outer radius $r = b$, *viz.,*

$$\mathcal{M}_t = 0\,, \qquad \bar{V}_n = \frac{2F}{b}\sin 4\theta\,, \tag{4.3}$$

where $F > 0$ is the total force of the traction over the interval $\theta \in [\,0\,,\ \pi/4\,]$.

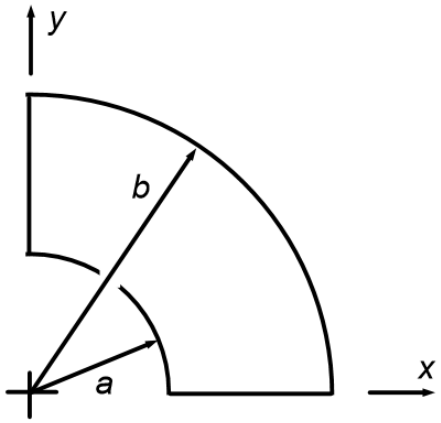

Figure 2. The quarter-annular plate under consideration.

This problem may be solved with a displacement of the form

$$u = f(r)\sin 4\theta\,. \tag{4.4}$$

With eqn. (4.4) and the first of eqns. (1.10), the components of the rotation vector are

$$\phi_r = \frac{4}{r}\,f\cos 4\theta\,, \qquad \phi_\theta = -f'\sin 4\theta\,. \tag{4.5}$$

Next, via the second of eqns. (1.10) and Hooke's Law, the moments are

$$\begin{aligned} M_{rr} &= -M_{\theta\theta} = \frac{Eh^3}{3(1+\nu)}\left(\frac{1}{r}f' - \frac{1}{r^2}f\right)\cos 4\theta, \\ M_{r\theta} &= -\frac{Eh^3}{12(1-\nu^2)}\left(f'' + \frac{\nu}{r}f' - \frac{16\nu}{r^2}f\right)\sin 4\theta\,, \\ M_{\theta r} &= \frac{Eh^3}{12(1-\nu^2)}\left(\nu f'' + \frac{1}{r}f' - \frac{16}{r^2}f\right)\sin 4\theta\,. \end{aligned} \tag{4.6}$$

Finally, eqn. (1.11) gives the components of the shear vector

$$\begin{aligned} V_r &= -\frac{Eh^3}{12(1-\nu^2)}\left(f''' + \frac{1}{r}f'' - \frac{17}{r^2}f' + \frac{32}{r^3}f\right)\sin 4\theta\,, \\ V_\theta &= -\frac{Eh^3}{3(1-\nu^2)}\left(\frac{1}{r}f'' + \frac{1}{r^2}f' - \frac{16}{r^3}f\right)\cos 4\theta\,. \end{aligned} \tag{4.7}$$

On the boundary, the Kirchhoff shear forces are

$$\begin{aligned} &r = b \ \Rightarrow\ \bar{V}_n = V_r - \frac{1}{r}\frac{\mathrm{d}M_{rr}}{\mathrm{d}\theta}\,, \qquad \theta = 0 \ \Rightarrow\ \bar{V}_n = -V_\theta - \frac{\mathrm{d}M_{\theta\theta}}{\mathrm{d}r}\,, \\ &\theta = \pi/2 \ \Rightarrow\ \bar{V}_n = V_\theta + \frac{\mathrm{d}M_{\theta\theta}}{\mathrm{d}r}\,, \qquad r = a \ \Rightarrow\ \bar{V}_n = -V_r + \frac{1}{r}\frac{\mathrm{d}M_{rr}}{\mathrm{d}\theta}\,, \end{aligned} \tag{4.8}$$

or, respectively, for $r = b$, $\theta = 0$, $\theta = \pi/2$ and $r = a$,

$$\begin{aligned} \bar{V}_n &= -\frac{Eh^3}{12(1-\nu^2)}\left[f''' + \frac{1}{b}f'' - \frac{(33-16\nu)}{b^2}f' + \frac{16(3-\nu)}{b^3}f\right]\sin 4\theta\,, \\ \bar{V}_n &= \frac{Eh^3}{12(1-\nu^2)}\left[\frac{4(2-\nu)}{r}f'' - \frac{4(1-2\nu)}{r^2}f' - \frac{8(7+\nu)}{r^3}f\right], \end{aligned}$$

$$\bar{V}_n = -\frac{Eh^3}{12(1-\nu^2)}\left[\frac{4(2-\nu)}{r}f'' - \frac{4(1-2\nu)}{r^2}f' - \frac{8(7+\nu)}{r^3}f\right], \tag{4.9}$$

$$\bar{V}_n = \frac{Eh^3}{12(1-\nu^2)}\left[f''' + \frac{1}{a}f'' - \frac{(33-16\nu)}{a^2}f' + \frac{16(3-\nu)}{a^3}f\right]\sin 4\theta\,.$$

Now, substituting the displacement (4.4) into the governing equation $\nabla^4 u = 0$, see eqn. (1.12), one obtains the differential equation

$$f'''' + \frac{2}{r}f''' - \frac{33}{r^2}f'' + \frac{33}{r^3}f' + \frac{192}{r^4}f = 0\,. \tag{4.10}$$

The solution to eqn. (4.10) is

$$\begin{aligned} f &= \frac{k_1}{r^4} + \frac{k_2}{r^2} + k_3 r^4 + k_4 r^6\,, \\ f' &= -4\frac{k_1}{r^5} - 2\frac{k_2}{r^3} + 4k_3 r^3 + 6k_4 r^5\,, \\ f'' &= 20\frac{k_1}{r^6} + 6\frac{k_2}{r^4} + 12k_3 r^2 + 30k_4 r^4\,, \\ f''' &= -120\frac{k_1}{r^7} - 24\frac{k_2}{r^5} + 24k_3 r + 120k_4 r^3\,. \end{aligned} \tag{4.11}$$

Looking at eqns. (4.4) and (4.6), one sees that the boundary conditions (4.1) are satisfied identically. The conditions, respectively, $u(a,\theta) = 0$, $\phi_t = -\phi_\theta(a,\theta) = 0$, $\mathcal{M}_t = M_{r\theta}(b,\theta) = 0$ and $\bar{V}_n = (2F/b)\sin 4\theta$ yield the system of equations to satisfy the boundary conditions (4.2) and (4.3), *viz.,*

$$\begin{bmatrix} 1/a^4 & 1/a^2 & a^4 & a^6 \\ -2/a^5 & -1/a^3 & 2a^3 & 3a^5 \\ 10(1-\nu)/b^6 & 3(1-3\nu)/b^4 & 6(1-\nu)b^2 & 5(3-\nu)b^4 \\ -5(1-\nu)/b^6 & -3(2-\nu)/b^4 & 3(1-\nu)b^2 & -5\nu b^4 \end{bmatrix}\begin{bmatrix} k_1 \\ k_2 \\ k_3 \\ k_4 \end{bmatrix} = \begin{bmatrix} 0 \\ 0 \\ 0 \\ 3(1-\nu^2)F/(2Eh^3) \end{bmatrix}. \tag{4.12}$$

Using the constants

$$E = 3.0\times 10^7 \text{ psi}\,,\quad \nu = 0.3\,,\quad h = 1.0 \text{ in}\,,\quad F = 10\,000 \text{ lb}\,,\quad a = 120 \text{ in}\,,\quad b = 360 \text{ in}\,, \tag{4.13}$$

the solution to eqn. (4.12) is

$$\begin{aligned} k_1 &= 1.666\,591\,940\,231\,4806\times 10^8\,, & k_2 &= -1.547\,802\,450\,020\,5023\times 10^4\,, \\ k_3 &= 1.354\,435\,354\,756\,7996\times 10^{-9}\,, & k_4 &= -3.252\,532\,373\,598\,9290\times 10^{-15} \end{aligned} \tag{4.14}$$

which constants solve the problem at hand.

As a final comment, for the constants (4.13) and (4.14), the values of the four corner forces are

Corner Force at (r,θ)	Value (lb)
$(M_{\theta\theta} - M_{rr})(a,0)$	0
$(M_{\theta\theta} - M_{rr})(b,0)$	−3935.94
$(M_{rr} - M_{\theta\theta})(b,\pi/2)$	3935.94
$(M_{rr} - M_{\theta\theta})(a,\pi/2)$	0

5. A C_1 18–Degree of Freedom Triangle Element

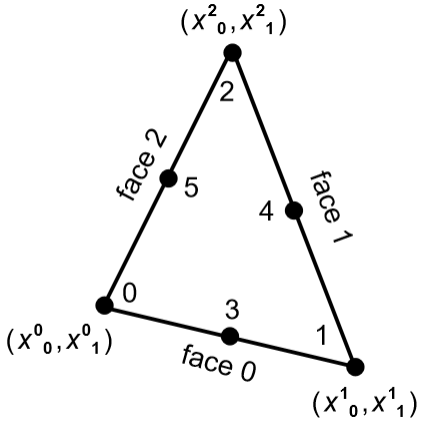

Figure 3. The 21–degree of freedom triangle as explained in the text.

At left, in Fig. 3, is shown a 21–degree of freedom triangle finite element. The vertex nodes 0, 1 and 2 each possess six degrees of freedom, *viz.,* u, $u_{,x}$, $u_{,y}$, $u_{,xx}$, $u_{,xy}$ and $u_{,yy}$. The three face nodes 3, 4 and 5 are located at the face midpoints, and they each possess a single degree of freedom $u_{,n}$, *i.e.,* the normal derivative in the outward direction. Denoting the 21 degrees of freedom as u^I, which is the element displacement vector, the displacement u in the interior of the element is interpolated via

$$u = S^I u^I \ , \tag{5.1}$$

where S^I are the so-called shape functions. The shape functions may be written as

$$S^I = b^{IJ} t^J \qquad (I,J) \in (0,20) \ , \tag{5.2}$$

where t^J are the terms of the complete fifth-order polynomial, *i.e.,*

$$t^J = \begin{bmatrix} t^0 & & & & & \\ t^1 & t^2 & & & & \\ t^3 & t^4 & t^5 & & & \\ t^6 & t^7 & t^8 & t^9 & & \\ t^{10} & t^{11} & t^{12} & t^{13} & t^{14} & \\ t^{15} & t^{16} & t^{17} & t^{18} & t^{19} & t^{20} \end{bmatrix} = \begin{bmatrix} 1 & & & & & \\ x & y & & & & \\ x^2 & xy & y^2 & & & \\ x^3 & x^2y & xy^2 & y^3 & & \\ x^4 & x^3y & x^2y^2 & xy^3 & y^4 & \\ x^5 & x^4y & x^3y^2 & x^2y^3 & xy^4 & y^5 \end{bmatrix} . \tag{5.3}$$

The matrix of coefficients b^{IJ} in eqn. (5.2) is found by inverting a 21×21 matrix. In practice, the coordinates in eqn. (5.3) are translated so that node 0 is at the origin, which avoids any numerical ill-conditioning.

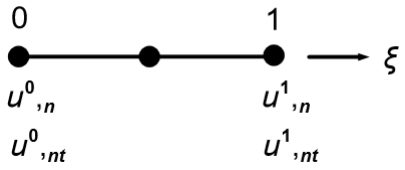

Figure 4. A cubic variation of $u_{,n}$ along a face of the triangle.

The three mid-side nodes are somewhat of a nuisance, so these three degrees of freedom are removed from the element by using the following procedure. The normal derivative is assumed to be cubic along the faces of the element, *i.e.,*

$$u_{,n} = f^0 u^0_{,n} + f^1 u^0_{,nt} + f^2 u^1_{,n} + f^3 u^1_{,nt} \ , \tag{5.4}$$

where the derivatives are in the boundary nt–system, and

$$f^0 = \frac{1}{4}(2 - 3\xi + \xi^3) \ , \qquad f^1 = \frac{L}{8}(1 - \xi - \xi^2 + \xi^3) \ ,$$
$$f^2 = \frac{1}{4}(2 + 3\xi - \xi^3) \ , \qquad f^3 = \frac{L}{8}(-1 - \xi + \xi^2 + \xi^3) \ . \tag{5.5}$$

In eqns. (5.5), $\xi \in (-1,1)$ is the normalized coordinate along the element face, as pictured in Fig. 4. The length of the element face is L. Evaluating eqns. (5.5) at $\xi = 0$, *i.e.,* at the mid-node,

$$f^0 = \frac{1}{2} \ , \qquad f^1 = \frac{L}{8} \ , \qquad f^2 = \frac{1}{2} \ , \qquad f^3 = -\frac{L}{8} \ , \tag{5.6}$$

and using $u_{,n} = n_i u_{,i}$ and $u_{,nt} = n_i t_j u_{,ij}$ (**n** and **t** are the unit normal and tangent vectors), one obtains that

$$u^{18} = A^{18\,I} u^I \ , \qquad u^{19} = A^{19\,I} u^I \ , \qquad u^{20} = A^{20\,I} u^I \ , \qquad I \in (0,17) \tag{5.7}$$

where 18, 19, and 20 are the degree of freedom numbers of the mid-node normal derivates, and

$$A^{18\,I} = \begin{bmatrix} 0 \\ n_x^0/2 \\ n_y^0/2 \\ L^0 n_x^0 t_x^0/8 \\ L^0\left(n_x^0 t_y^0 + n_y^0 t_x^0\right)/8 \\ L^0 n_y^0 t_y^0/8 \\ 0 \\ n_x^0/2 \\ n_y^0/2 \\ -L^0 n_x^0 t_x^0/8 \\ -L^0\left(n_x^0 t_y^0 + n_y^0 t_x^0\right)/8 \\ -L^0 n_y^0 t_y^0/8 \\ 0 \\ 0 \\ 0 \\ 0 \\ 0 \\ 0 \end{bmatrix}, \quad A^{19\,I} = \begin{bmatrix} 0 \\ 0 \\ 0 \\ 0 \\ 0 \\ 0 \\ 0 \\ n_x^1/2 \\ n_y^1/2 \\ L^1 n_x^1 t_x^1/8 \\ L^1\left(n_x^1 t_y^1 + n_y^1 t_x^1\right)/8 \\ L^1 n_y^1 t_y^1/8 \\ 0 \\ n_x^1/2 \\ n_y^1/2 \\ -L^1 n_x^1 t_x^1/8 \\ -L^1\left(n_x^1 t_y^1 + n_y^1 t_x^1\right)/8 \\ -L^1 n_y^1 t_y^1/8 \end{bmatrix}, \quad A^{20\,I} = \begin{bmatrix} 0 \\ n_x^2/2 \\ n_y^2/2 \\ -L^2 n_x^2 t_x^2/8 \\ -L^2\left(n_x^2 t_y^2 + n_y^2 t_x^2\right)/8 \\ -L^2 n_y^2 t_y^2/8 \\ 0 \\ 0 \\ 0 \\ 0 \\ 0 \\ 0 \\ 0 \\ n_x^2/2 \\ n_y^2/2 \\ L^2 n_x^2 t_x^2/8 \\ L^2\left(n_x^2 t_y^2 + n_y^2 t_x^2\right)/8 \\ L^2 n_y^2 t_y^2/8 \end{bmatrix} . \quad (5.8)$$

In eqns. (5.8) the superscripts on L, n_x, n_y, t_x and t_y refer to the face numbers in Fig. 3. Finally, via eqns. (5.7) and (5.8), the interpolation and shape functions become

$$u = S^I u^I \ , \qquad S^I = c^{IJ} t^J \ , \qquad I \in (0{,}17) \ , \qquad J \in (0{,}20) \ ,$$
$$c^{IJ} = b^{IJ} + A^{18\,I} b^{18\,J} + A^{19\,I} b^{19\,J} + A^{20\,I} b^{20\,J} \ . \quad (5.9)$$

Thus, with eqns. (5.9), the element now only has nodes at the vertices, leaving an 18−degree of freedom element. Finally, note that the gradients of u are interpolated as

$$u_{,i} = S^I_{,i} u^I \ , \qquad u_{,ij} = S^I_{,ij} u^I \ , \qquad S^I_{,i} = c^{IJ} t^J_{,i} \ , \qquad S^I_{,ij} = c^{IJ} t^J_{,ij} \ , \qquad \text{etc.} \quad (5.10)$$

Turning attention to the Principle of Virtual Work (2.9), interpolate the virtual displacement u^* and virtual rotation ϕ_i^* as

$$u^* = S^I u^{*I} \ , \qquad \phi_i^* = \varepsilon_{ik} u^*_{,k} = \varepsilon_{ik} S^I_{,k} u^{*I} \quad \Rightarrow \quad \phi_t^* = t_i \phi_i^* = t_i \varepsilon_{ik} S^I_{,k} u^{*I} \ , \quad (5.11)$$

where u^{*I} are the nodal values of u^*. Substitution of the interpolations (5.11) into eqn. (2.9) yields

$$u^{*I} \int_A S^I_{,kj} C_{jkpq} u_{,qp} \, \mathrm{d}A = u^{*I} \oint_t t_i \varepsilon_{ik} S^I_{,k} \mathcal{M}_t \, \mathrm{d}t + u^{*I} \oint_t S^I \bar{V}_n \, \mathrm{d}t + u^{*I} \int_A S^I q \, \mathrm{d}A \ , \quad (5.12)$$

or since u^{*I} is arbitrary

$$\int_A S^I_{,kj} C_{jkpq} u_{,qp} \, \mathrm{d}A = \oint_t t_i \varepsilon_{ik} S^I_{,k} \mathcal{M}_t \, \mathrm{d}t + \oint_t S^I \bar{V}_n \, \mathrm{d}t + \int_A S^I q \, \mathrm{d}A \ . \quad (5.13)$$

Now, putting the interpolations $u_{,qp} = S^J_{,qp} u^J$ into eqn. (5.13) gives the element stiffness relation

$$K^{IJ} u^J = f^I_{\mathcal{M}} + f^I_V + f^I_q = f^I \ , \quad (5.14)$$

where

$$K^{IJ} = \int_A S^I_{,kj} C_{ijpq} S^J_{,qp} \, \mathrm{d}A \ , \qquad f^I_{\mathcal{M}} = \oint_t t_i \varepsilon_{ik} S^I_{,k} \mathcal{M}_t \, \mathrm{d}t \ , \qquad f^I_V = \oint_t S^I \bar{V}_n \, \mathrm{d}t \ , \qquad f^I_q = \int_A S^I q \, \mathrm{d}A \ . \quad (5.15)$$

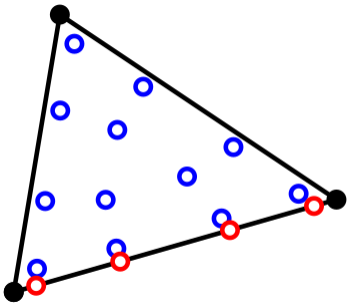

Figure 5. Quadrature points. The blue points are for area integrations and the red points are for linear boundary integrations.

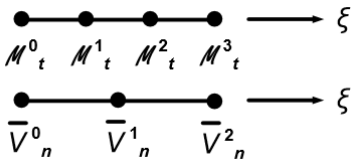

Figure 6. Schematic of prescribed non-zero boundary values of $\mathcal{M}_t$ and $\bar{V}_n$.

The area integrals in eqns. (5.15) are calculated numerically with the 12-point quadrature rule of Dunavant, the quadrature points of which rule are depicted by the blue points in Fig. 5 above. The 12-point rule will integrate a sixth-order polynomial exactly. In the integral expression for f^I_q, q is interpolated through the element area via $q = N^I q^I$, where q^I are the three nodal values of q, and N^I are the usual linear shape functions (based on area coordinates) of the triangle. The linear integrations (along the boundaries) in eqns. (5.15) are performed using the 4-point Gauss-Legendre quadrature rule, which rule will integrate a seventh order polynomial exactly. The quadrature points for this rule are depicted by the red points above in Fig. 5.

Figure 6 above shows an element face where non-zero boundary values of $\mathcal{M}_t$ and/or $\bar{V}_n$ are prescribed, where $\xi \in (-1,1)$ is the normalized coordinate along the element face. If $\mathcal{M}_t$ is prescribed, then it is represented by the cubic function

$$\mathcal{M}_t = m^0 \mathcal{M}^0_t + m^1 \mathcal{M}^1_t + m^2 \mathcal{M}^2_t + m^3 \mathcal{M}^3_t \ , \quad (5.16)$$

where $\mathcal{M}^I_t$ are the values of $\mathcal{M}_t$ at four equally spaced points along the element face (as depicted in Fig. 6), and

$$m^0 = \frac{1}{16}(-1 + \xi + 9\xi^2 - 9\xi^3) \ , \qquad m^1 = \frac{9}{16}(1 - 3\xi - \xi^2 + 3\xi^3) \ ,$$
$$m^2 = \frac{9}{16}(1 + 3\xi - \xi^2 - 3\xi^3) \ , \qquad m^3 = \frac{1}{16}(-1 - \xi + 9\xi^2 + 9\xi^3) \ . \quad (5.17)$$

Similarly, if $\bar{V}_n$ is prescribed, then it is represented by the quadratic function

$$\bar{V}_n = v^0 \bar{V}^0_n + v^1 \bar{V}^1_n + v^2 \bar{V}^2_n \ , \quad (5.18)$$

where $\bar{V}^I_n$ are the values of $\bar{V}_n$ at three equally spaced points along the element face, and

$$v^0 = \frac{1}{2}(-\xi + \xi^2) \ , \qquad v^1 = 1 - \xi^2 \ , \qquad v^2 = \frac{1}{2}(\xi + \xi^2) \ . \quad (5.19)$$

At this point, it is worth demonstrating that this element exhibits C_1 continuity, *i.e.,* the value of $u_{,n}$ is continuous across adjoining elements. If an element does not possess C_1 continuity, then numerical results obtained for plate theory will not converge to the exact solution. This is because the integrand in the first integral of eqns. (5.13) is not defined on the boundaries of the element. Notwithstanding, Fig. 7 below shows two adjoining triangle elements. In the figure: the red numbers are the element numbers; the blue numbers are the element local node numbers; and the black numbers, the global node numbers. A global displacement vector $\mathbf{u}^g$,

$$\mathbf{u}^g = \begin{bmatrix} 23 \\ 15 \\ 16 \\ 21 \\ 13 \\ 2 \\ 10 \\ 12 \\ 24 \\ 5 \\ 8 \\ 14 \\ 4 \\ 11 \\ 19 \\ 6 \\ 3 \\ 7 \\ 9 \\ 17 \\ 20 \\ 18 \\ 22 \\ 1 \end{bmatrix}$$

shown in Fig. 8, was applied to the assemblage of two elements. It contains the integers 1 through 24 listed in random order. Figure 9 below shows the variation of u along the line running from global node 1 to global node 2. The solid red curve is obtained with the shape functions of element 0; and the dashed blue curve, with the shape functions of element 1. The two curves coincide, *i.e.,* the element is C_0 continuous. Figure 10 below shows the variation of the normal derivative $u_{,n}$ along

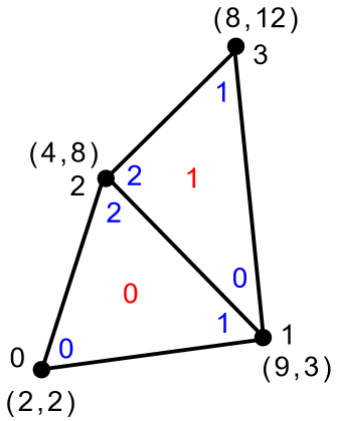

Figure 7 (directly above). An assembly of two triangle elements as explained in the text.

Figure 8 (at left). The global displacement vector applied to the assemblage of elements in Fig. 7.

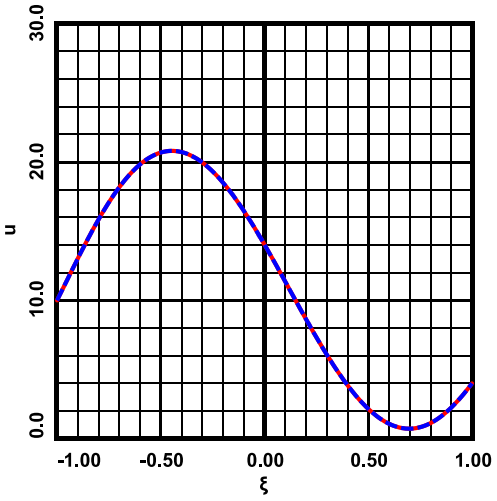

Figure 9. Variation of u along the adjoining boundary of the two elements, as described in the text.

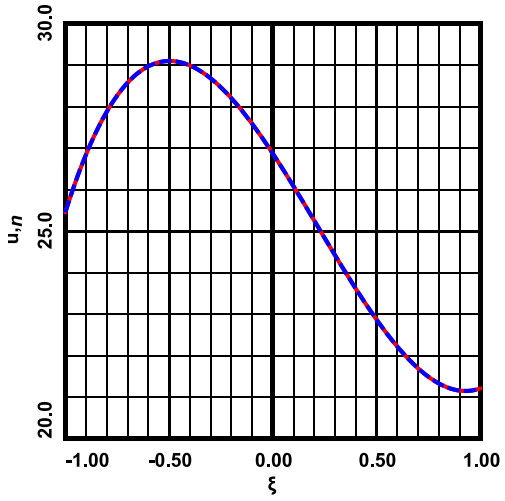

Figure 10. Variation of $u_{,n}$ along the adjoining boundary of the two elements, as described in the text.

the line running from global node 1 to global node 2. The direction of the normal derivative is from element 0 to element 1. Once again, the solid red curve is obtained with the shape functions of element 0; and the dashed blue curve, with those of element 1. The two curves coincide, *i.e.,* the element is C_1 continuous.

6. A C_1 24–Degree of Freedom Quadrilateral Element

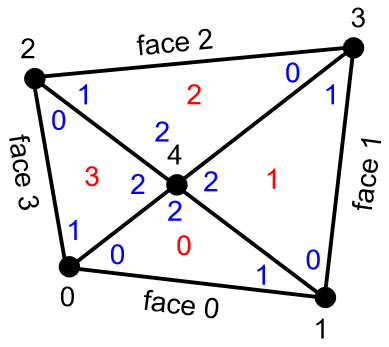

Figure 11. Quadrilateral element as described in the text.

At left, in Fig. 11, is shown a 30–degree of freedom quadrilateral element, which, in fact, is just an assemblage of four triangle elements. The central node is at the intersection of the quadrilateral's diagonals, and in the figure: the black numbers are the local node numbers of the quadrilateral; the blue numbers, the local node numbers of the triangles; and the red numbers, the triangle numbers. The quadrilateral stiffness relation is then the assembly of the four triangle's stiffness relations. To remove the central node 4, write the quadrilateral stiffness relation in terms of sub-matrices

$$\begin{bmatrix} \mathbf{K}_{24\times24} & \mathbf{L}_{24\times6} \\ \mathbf{M}_{6\times24} & \mathbf{N}_{6\times6} \end{bmatrix} \begin{bmatrix} \mathbf{u}_{24\times1} \\ \mathbf{v}_{6\times1} \end{bmatrix} = \begin{bmatrix} \mathbf{f}_{24\times1} \\ \mathbf{g}_{6\times1} \end{bmatrix} , \tag{6.1}$$

where $\mathbf{v}_{6\times1}$ contains the displacement degrees of freedom of the central node. Solving for $\mathbf{v}$, one obtains

$$\mathbf{w} = \mathbf{N}^{-1}\mathbf{g} , \qquad \mathbf{P} = \mathbf{N}^{-1}\mathbf{M} \quad \Rightarrow \quad \mathbf{v} = \mathbf{w} - \mathbf{P}\mathbf{u} . \tag{6.2}$$

Substituting this expression for $\mathbf{v}$ back into eqn. (6.1) gives

$$\mathbf{Q} = \mathbf{L}\mathbf{P} , \qquad \mathbf{z} = \mathbf{L}\mathbf{w} \quad \Rightarrow \quad [\,\mathbf{K} - \mathbf{Q}\,]\,\mathbf{u} = \mathbf{f} - \mathbf{z} , \tag{6.3}$$

the last equation of which is the 24×24 stiffness relation of the four-noded quadrilateral element (again, with the central node removed).

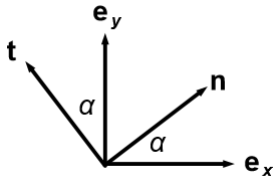

Figure 12. The xy– and nt–systems.

Sometimes, to apply the displacement boundary conditions of the problem, a node will need to be transformed from the xy–system to the boundary nt–system. The unit vectors in Fig. 12 at left are

$$\begin{aligned} \mathbf{n} &= \cos\alpha\,\mathbf{e}_x + \sin\alpha\,\mathbf{e}_y = n_x\mathbf{e}_x + n_y\mathbf{e}_y \\ \mathbf{t} &= -\sin\alpha\,\mathbf{e}_x + \cos\alpha\,\mathbf{e}_y = t_x\mathbf{e}_x + t_y\mathbf{e}_y . \end{aligned} \tag{6.4}$$

Now, define the matrices $\mathbf{T}^1$, $\mathbf{T}^2$ and $\mathbf{T}$ in terms of the unit vectors $\mathbf{n}$ and $\mathbf{t}$ of eqn. (6.4) via

$$\mathbf{T}^1 = \begin{bmatrix} n_x & n_y \\ t_x & t_y \end{bmatrix} , \qquad \mathbf{T}^2 = \begin{bmatrix} n_x^2 & 2n_xn_y & n_y^2 \\ n_xt_x & n_xt_y + n_yt_x & n_yt_y \\ t_x^2 & 2t_xt_y & t_y^2 \end{bmatrix} , \qquad \mathbf{T} = \begin{bmatrix} 1_{1\times1} & \mathbf{0}_{1\times2} & \mathbf{0}_{1\times3} \\ \mathbf{0}_{2\times1} & \mathbf{T}^1_{2\times2} & \mathbf{0}_{2\times3} \\ \mathbf{0}_{3\times1} & \mathbf{0}_{3\times2} & \mathbf{T}^2_{3\times3} \end{bmatrix} \tag{6.5}$$

so that the nodal transformations between the two coordinate systems are

$$\mathbf{u}_{nt} = \mathbf{T}\mathbf{u}_{xy} , \qquad \mathbf{u}_{xy} = \mathbf{T}^{-1}\mathbf{u}_{nt} . \tag{6.6}$$

In eqns. (6.6), $\mathbf{u}_{xy}$ are the six displacement components of a node in the xy–system, and $\mathbf{u}_{nt}$ are the six displacement components of a node in the nt–system. Next, write the stiffness relation (6.3) of the quadrilateral in terms of 6×6 and 6×1 submatrices as

$$\begin{bmatrix} \mathbf{K}^{00} & \mathbf{K}^{01} & \mathbf{K}^{02} & \mathbf{K}^{03} \\ \mathbf{K}^{10} & \mathbf{K}^{11} & \mathbf{K}^{12} & \mathbf{K}^{13} \\ \mathbf{K}^{20} & \mathbf{K}^{21} & \mathbf{K}^{22} & \mathbf{K}^{23} \\ \mathbf{K}^{30} & \mathbf{K}^{31} & \mathbf{K}^{32} & \mathbf{K}^{33} \end{bmatrix} \begin{bmatrix} \mathbf{u}^0_{xy} \\ \mathbf{u}^1_{xy} \\ \mathbf{u}^2_{xy} \\ \mathbf{u}^3_{xy} \end{bmatrix} = \begin{bmatrix} \mathbf{f}^0_{xy} \\ \mathbf{f}^1_{xy} \\ \mathbf{f}^2_{xy} \\ \mathbf{f}^3_{xy} \end{bmatrix} . \tag{6.7}$$

Finally, for example, if node 1 of the element is in the nt–system, then eqn. (6.7) is transformed as

$$\begin{bmatrix} \mathbf{K}^{00} & \mathbf{K}^{01}\mathbf{T}^{-1} & \mathbf{K}^{02} & \mathbf{K}^{03} \\ \mathbf{T}^{-T}\mathbf{K}^{10} & \mathbf{T}^{-T}\mathbf{K}^{11}\mathbf{T}^{-1} & \mathbf{T}^{-T}\mathbf{K}^{12} & \mathbf{T}^{-T}\mathbf{K}^{13} \\ \mathbf{K}^{20} & \mathbf{K}^{21}\mathbf{T}^{-1} & \mathbf{K}^{22} & \mathbf{K}^{23} \\ \mathbf{K}^{30} & \mathbf{K}^{31}\mathbf{T}^{-1} & \mathbf{K}^{32} & \mathbf{K}^{33} \end{bmatrix} \begin{bmatrix} \mathbf{u}^0_{xy} \\ \mathbf{u}^1_{nt} \\ \mathbf{u}^2_{xy} \\ \mathbf{u}^3_{xy} \end{bmatrix} = \begin{bmatrix} \mathbf{f}^0_{xy} \\ \mathbf{f}^1_{nt} \\ \mathbf{f}^2_{xy} \\ \mathbf{f}^3_{xy} \end{bmatrix}, \tag{6.8}$$

where

$$\mathbf{f}^1_{nt} = \mathbf{T}^{-T}\mathbf{f}^1_{xy} \ . \tag{6.9}$$

7. Recovery of the Internal Force Resultants

The components of the moment tensor M_{ij} are readily calculated at the nodes from the nodal values of $u_{,xx}$, $u_{,xy}$ and $u_{,yy}$.

When calculating the components of the internal shear vector V_i, the usual approach would be to use the third gradients of the shape functions (5.9) in the interiors of the triangles. But, for some problems, especially ones which contain curved boundaries, the results can be unacceptably inaccurate. Consequently, here an alternate approach is used.

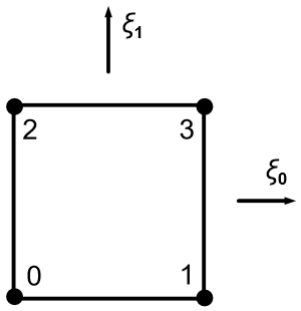

Figure 13. Differentiation cell in $\boldsymbol{\xi}$–space.

Figure 13 at left shows a bi-linear differentiation cell in normalized $\boldsymbol{\xi}$–space, with $\xi_i \in (-1,1)$. In physical $\mathbf{x}$–space, the cell corresponds to the quadrilateral element in Fig. 11. The shape functions S^I of the cell are

$$S^0 = f^0(\xi_0)f^0(\xi_1) \ , \qquad S^1 = f^1(\xi_0)f^0(\xi_1) \ ,$$
$$S^2 = f^0(\xi_0)f^1(\xi_1) \ , \qquad S^3 = f^1(\xi_0)f^1(\xi_1) \ , \tag{7.1}$$

where

$$f^0(\xi) = \frac{1}{2}(1-\xi) \ , \qquad f^1(\xi) = \frac{1}{2}(1+\xi) \ . \tag{7.2}$$

The mapping from $\boldsymbol{\xi}$–space to $\mathbf{x}$–space is given by

$$x_i = S^I x^I_i \ , \tag{7.3}$$

where x^I_i are the coordinates of the nodes. Now, from eqn. (7.3),

$$\frac{\partial x_i}{\partial \xi_\alpha} \equiv A_{i\alpha} = S^I_{,\alpha} x^I_i \quad \Rightarrow \quad \frac{\partial \xi_\alpha}{\partial x_i} = A^{-1}_{\alpha i} \ , \qquad S^I_{,i} = S^I_{,\alpha} A^{-1}_{\alpha i} \ . \tag{7.4}$$

Denoting the nodal values of the moment tensor as M^I_{ij}, interpolate M_{ij} within the cell as $M_{ij} = S^I M^I_{ij}$. Then eqns. (1.6) yield the components V_i, *viz.,*

$$V_x = S^I_{,x} M^I_{xy} + S^I_{,y} M^I_{yy} \ , \qquad V_y = -S^I_{,x} M^I_{xx} - S^I_{,y} M^I_{yx} \ . \tag{7.5}$$

8. Numerical Example in Cartesian Coordinates

Here the problem presented earlier in **§3** is solved numerically. Due to symmetry, only the upper right quadrant of Fig. 1 is analyzed. The (symmetry) boundary conditions at $x = 0$ and $y = 0$ are

$$\phi_t = 0 \ , \qquad \bar{V}_n = 0 \ . \tag{8.1}$$

On the boundaries $x = L/2$ and $y = H/2$ the (simply supported) boundary conditions are as per eqns. (3.3). The constants used in the analysis are

$$E = 3 \times 10^7 \text{ psi} \ , \quad \nu = 0.3 \ , \quad h = 1.0 \text{ in} \ , \quad L = 360 \text{ in} \ , \quad H = 240 \text{ in} \ , \quad F = 10000 \text{ lb} \ . \qquad (8.2)$$

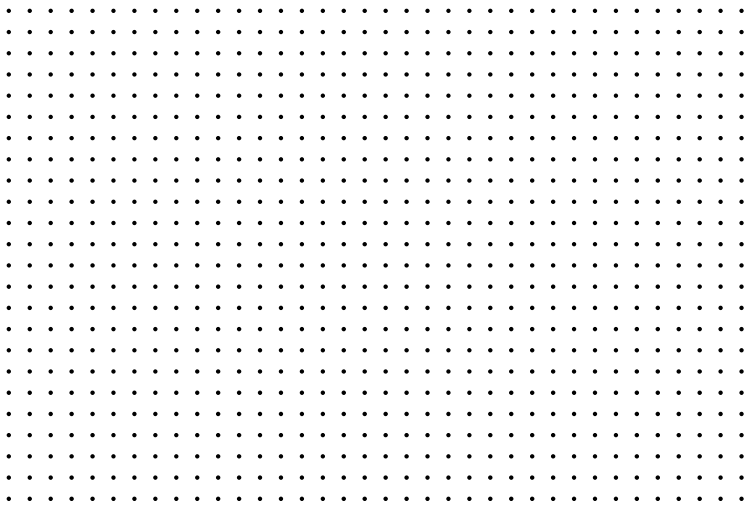

Figure 14. Grid used in the analysis as explained in the text.

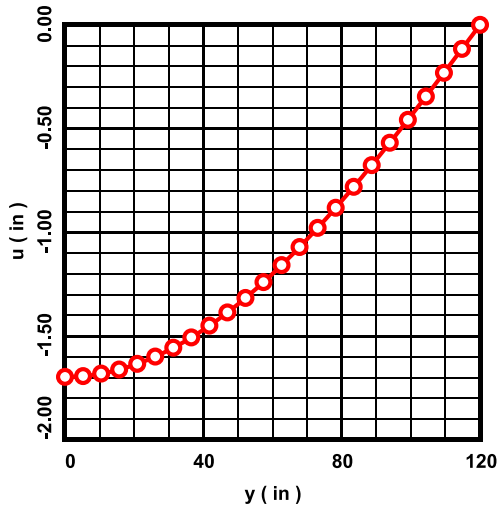

Figure 15. Results for the displacement u at $x = 0$.

The computational grid used in the analysis is pictured above in Fig. 14. It consists of a 36×24 array of nodes, and a 35×23 array of quadrilateral elements.

Figures 15 through 18 show the calculated results at (or near) the left boundary of the domain $x = 0$. In all graphs which follow: the solid curves represent the exact solution; and the plotted points, the numerical results. Figures 15 through 18 show, respectively, the results for the displacement, the rotation, the moment components, and shear vector. Note that in Fig. 18, the results are for a vertical line running through the centers of the leftmost column of elements, *i.e.,* for the vertical line at $x = 2.571$ in. In all cases, for all practicality, the numerical results reproduce the exact solution.

Figures 19 through 21 below show the results at (or near) the right boundary of the domain $x = 180$ in. These figures concern, respectively, the rotation, moment and shear vector. Also, the shear component in Fig. 21 is for a vertical line passing through the centers of the rightmost column of elements, *i.e.,* along the vertical line $x = 177.428$ in. As before, the numerical results basically reproduce the exact solution.

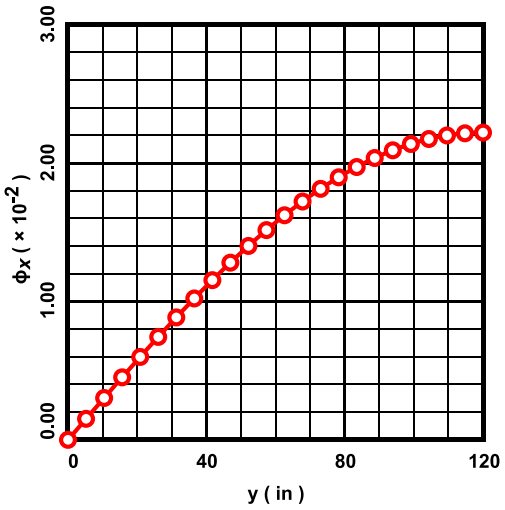

Figure 16. Results for the rotation component ϕ_x at $x = 0$.

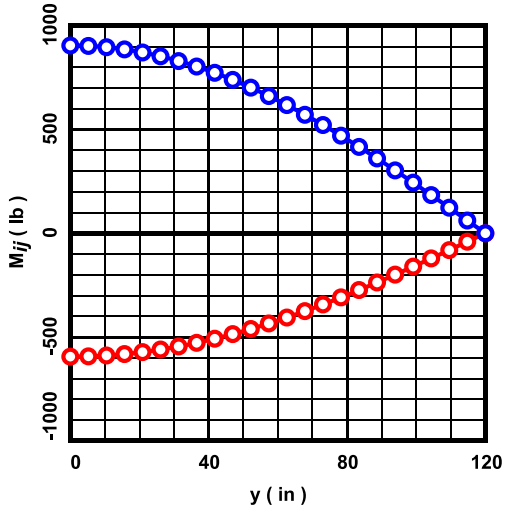

Figure 17. Results for the moment components M_{xy} (red) and M_{yx} (blue) at $x = 0$.

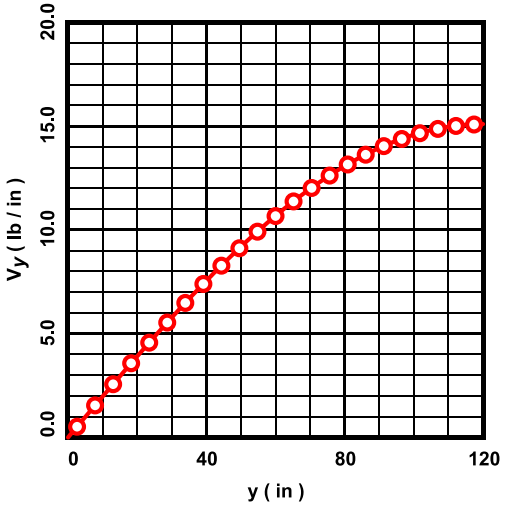

Figure 18. Results for the shear component V_y at $x = 2.571$ in.

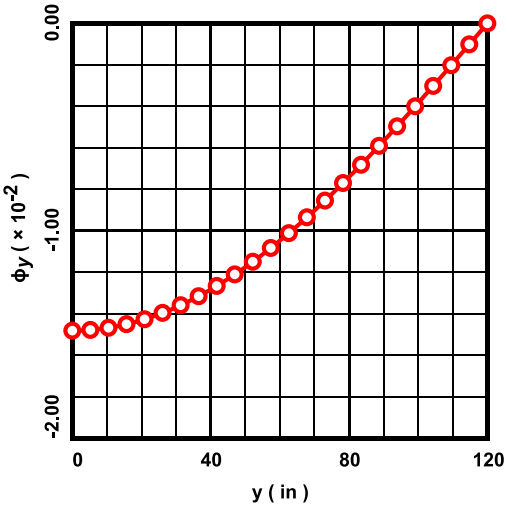

Figure 19. Results for the rotation component ϕ_y at $x = 180$ in.

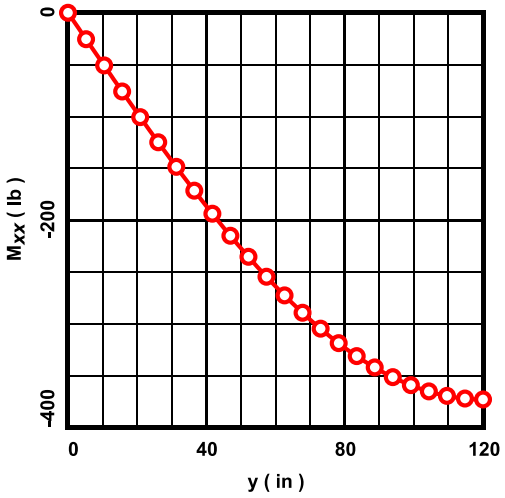

Figure 20. Results for the moment component M_{xx} at $x = 180$ in.

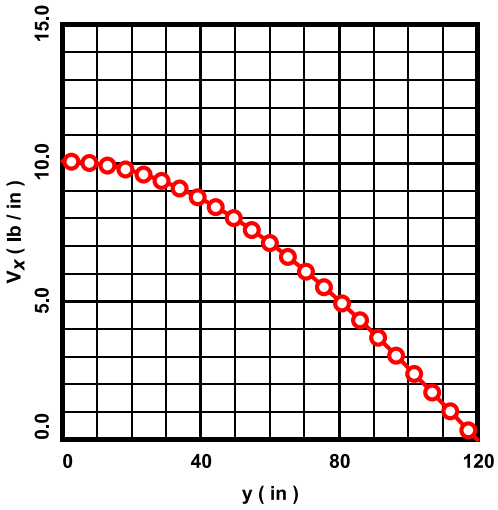

Figure 21. Results for the shear component V_x at $x = 177.428$ in.

Figures 22 through 24 below show the results for, respectively, the displacement u, the rotation vector ϕ_i and moment tensor M_{ij}, all along the vertical line of nodes in the grid located at $x = 82.286$ in. The results for the shear vector V_i in Fig. 25 are for the vertical line running through the centers of the column of elements located at $x = 84.857$ in. Once again, effectively, the numerical results reproduce the exact solution.

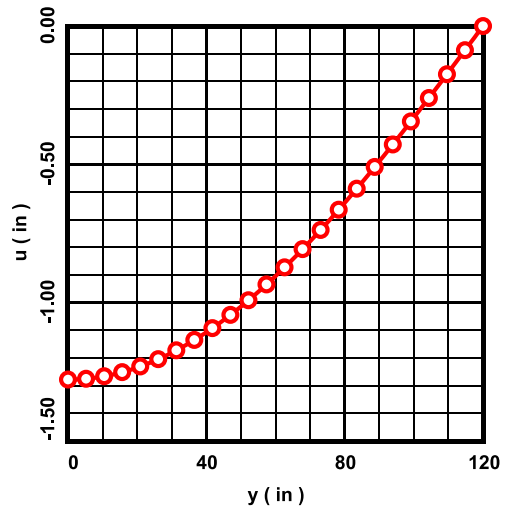

Figure 22. Results for the displacement u at $x = 82.286$ in.

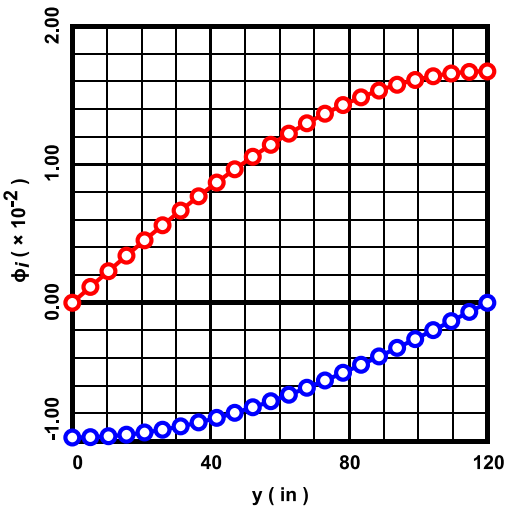

Figure 23. Results for the rotation components ϕ_x (red) and ϕ_y (blue) at $x = 82.286$ in.

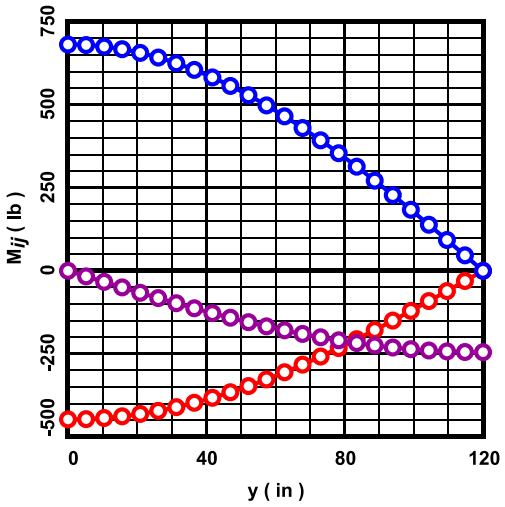

Figure 24. Results for the moment components M_{xy} (red), M_{yx} (blue) and M_{xx} (purple) at $x = 82.286$ in.

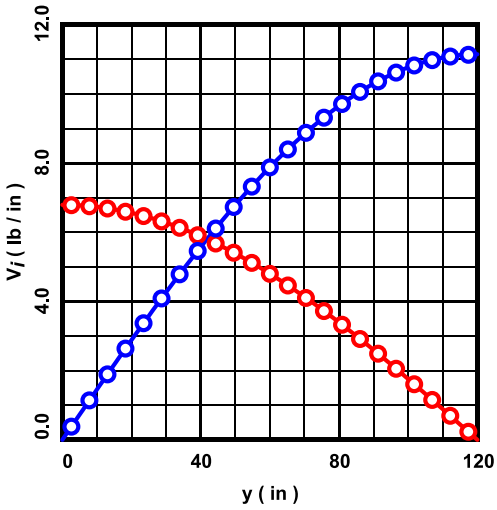

Figure 25. Results for the shear components V_x (red) and V_y (blue) at $x = 84.857$ in.

Finally, for the corner force located at the upper right corner of the domain, the numerically calculated value is -745.4 lb, while the exact value is -745.6 lb, *cf.,* eqn. (3.11), which amounts to a relative error of -0.027%.

9. Numerical Example in Polar Coordinates

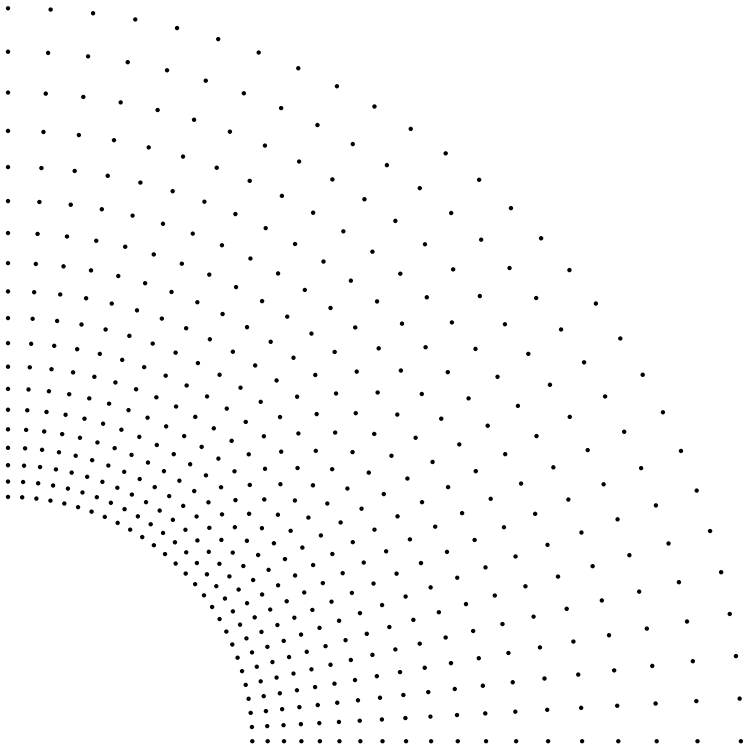

Figure 26. Computational grid used in the analysis, as explained in the text.

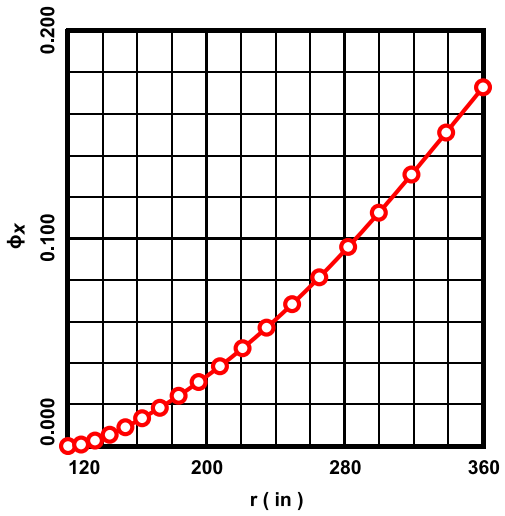

Figure 27. Results for rotation component ϕ_x at $\theta = 0$.

The problem solved earlier in **§4** is solved here numerically. The computational grid used in the analysis is shown above in Fig. 26. It consists of a 19 (radial) × 28 (tangential) array of nodes, and an 18 (radial) × 27 (tangential) array of quadrilateral elements. The constants used in the analysis are as per eqn. (4.13) above.

Figures 27 through 29 show the results at (or near) the boundary at $\theta = 0$. Figures 27 and 28 depict, respectively, the results for the rotation and moment at $\theta = 0$. Figure 29 depicts the shear vector along the radial line running through the centers of the elements at the bottom of the computational grid, *i.e.,* along $\theta = 0.009259\pi$. In all the graphs: the solid curves represent the exact solution; and the plotted points, the numerical solution. As is evident from Fig. 27, the numerical results for the rotation are quite accurate. The same is true for the moment (Fig.28), except for the slight error at the outer radius. Finally, for the shear component (Fig. 29), the numerical solution is also quite accurate, again, except for some minor error near the outer radius of the domain.

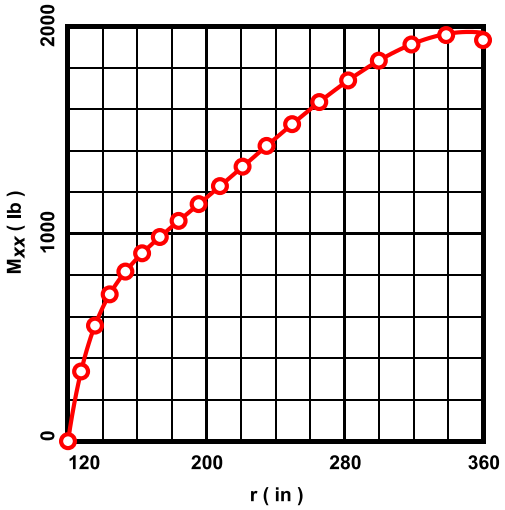

Figure 28. Results for moment component M_{xx} at $\theta = 0$.

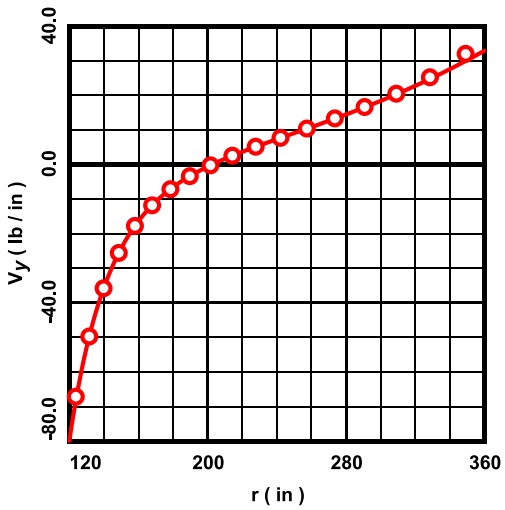

Figure 29. Results for shear component V_y at $\theta = 0.009259\pi$.

Figures 30 through 33 show the results for, respectively, the displacement u, the rotation vector ϕ_i, the moment tensor M_{ij} and shear vector V_i at (or near) the outer radius of the domain. The results in Figs. 30 through 32 correspond to the outer radius $r = 360$ in, while the results for the shear vector (Fig. 33) are for the circular arc running through the centers of the elements at the outer radius, *i.e.,* along the arc at $r = 349.2$ in. As is evident from Figs. 30 through 32, the numerical results for the displacement, rotations and moments are quite accurate. As for the shear vector (Fig. 33), while the numerically calculated values do exhibit some error, overall, though, their accuracy is still quite acceptable.

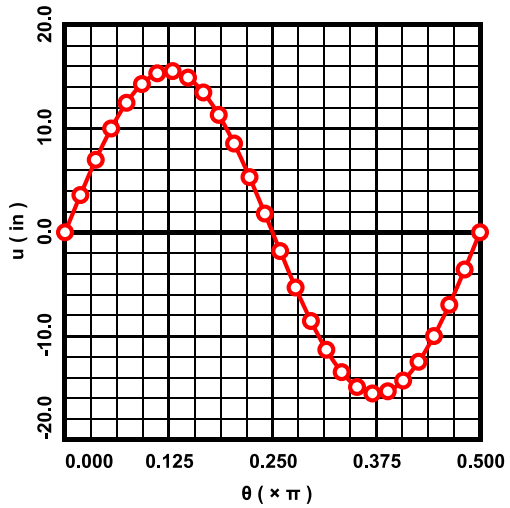

Figure 30. Results for displacement u at $r = 360$ in.

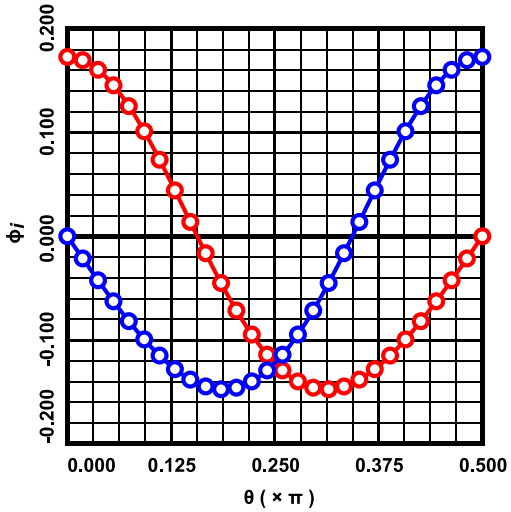

Figure 31. Results for rotation components ϕ_x (red) and ϕ_y (blue) at $r = 360$ in.

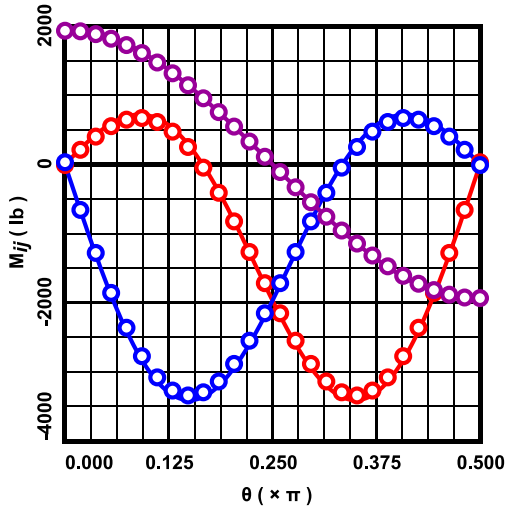

Figure 32. Results for moment components M_{xy} (red), M_{yx} (blue) and M_{xx} (purple) at $r = 360$ in.

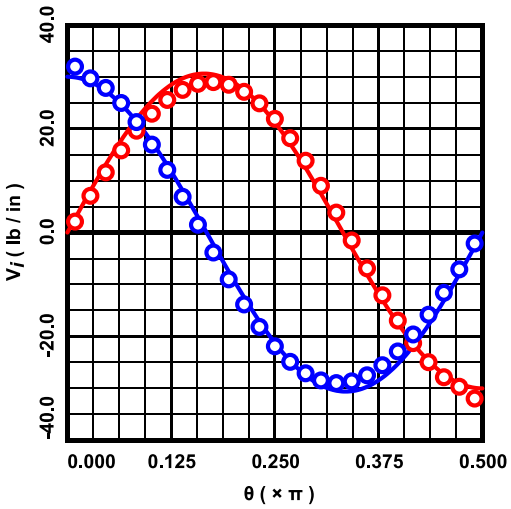

Figure 33. Results for shear components V_x (red) and V_y (blue) at $r = 349.2$ in.

Figures 34 and 35 below present the results for, respectively, the moment tensor M_{ij} at the inner radius of the domain $r = 120$ in, and the shear vector V_i along the circular arc running through the centers of the elements at the inner radius, *i.e.,* along $r = 123.7$ in. As is seen from Fig. 34, the magnitudes of the numerically calculated bending moments M_{xy} and M_{yx} are under-estimated somewhat. The numerically calculated shear components (Fig. 35) have generally the correct character, but the numerical results disagree with the exact solution by about 40% at $\theta \approx \pi/8$ (V_x) and $\theta \approx 3\pi/8$ (V_y). These results for the shear components V_i are the most inaccurate part of the solution, and the author considers them to be bordering on unacceptable.

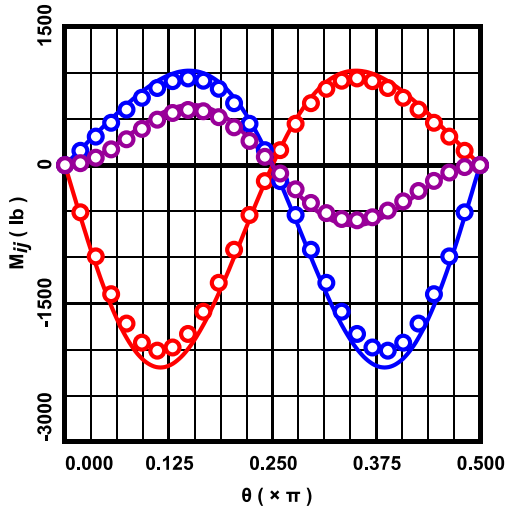

Figure 34. Results for moment components M_{xy} (red), M_{yx} (blue) and M_{xx} (purple) at $r = 120$ in.

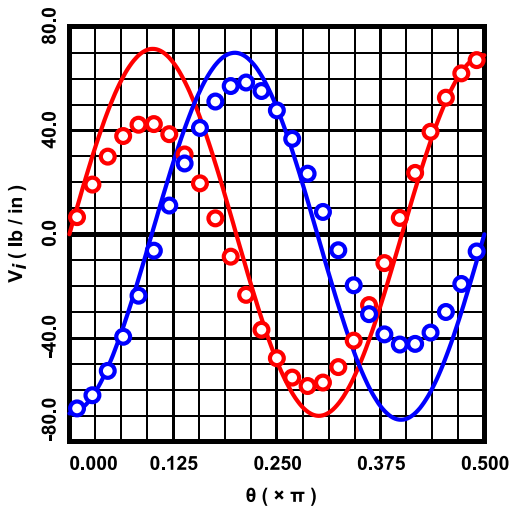

Figure 35. Results for shear components V_x (red) and V_y (blue) at $r = 123.7$ in.

Figures 36 through 38 below show the results for, respectively, the displacement u, the rotation vector ϕ_i and moment tensor M_{ij} along the radial line of nodes located at $\theta = 0.1296\pi$. Figure 39 shows the results for the shear vector V_i along the radial line passing through the centers of the quadrilateral elements located at inclination $\theta = 0.1204\pi$. As previously, the numerical results for u and ϕ_i are quite accurate. For the moments M_{ij} (Fig. 38), there is some slight inaccuracy at the inner and outer radii of the domain in the calculated bending moments M_{xy} and M_{yx}, but elsewhere the numerical results are quite accurate. As for the shear vector V_i (Fig. 39), in the interior of the domain the numerically calculated values are quite accurate and acceptable. Near the outer radius of the domain, though, there is some (somewhat minor) inaccuracy, but near the inner radius, the inaccuracy is very large (which is consistent with the results of Fig. 35 above).

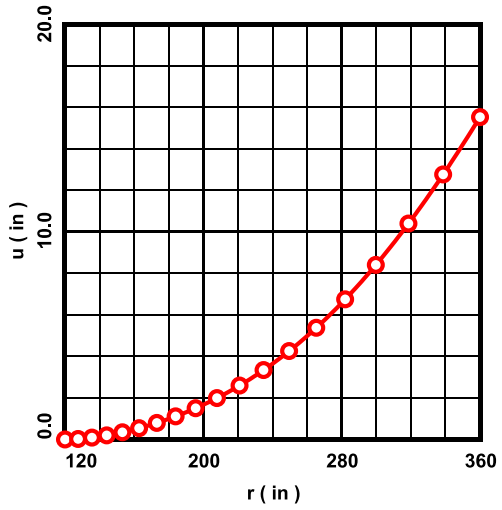

Figure 36. Results for displacement u at $\theta = 0.1296\pi$.

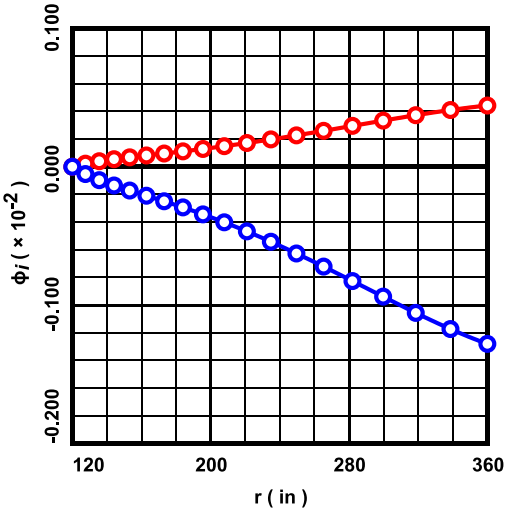

Figure 37. Results for rotation components ϕ_x (red) and ϕ_y (blue) at $\theta = 0.1296\pi$.

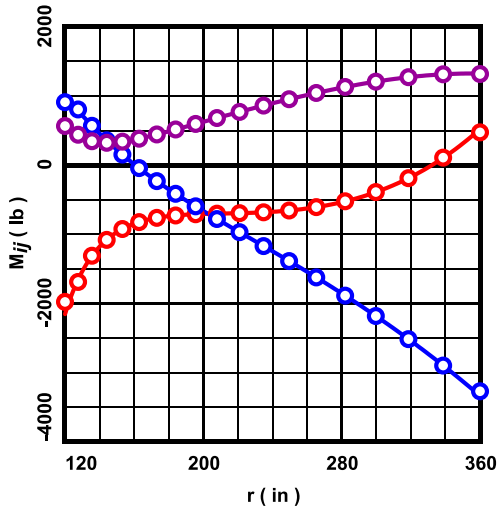

Figure 38. Results for moment components M_{xy} (red), M_{yx} (blue) and M_{xx} (purple) at $\theta = 0.1296\pi$.

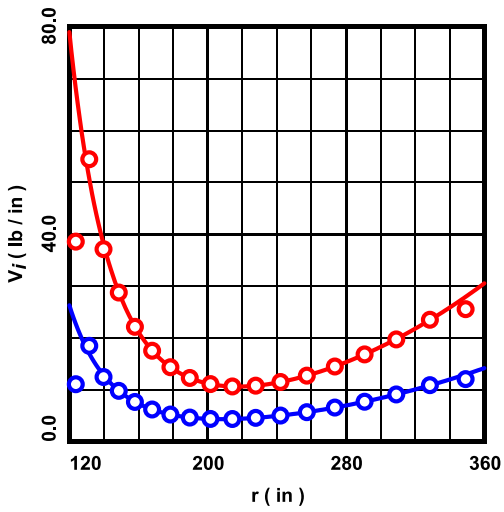

Figure 39. Results for shear components V_x (red) and V_y (blue) at $\theta = 0.1204\pi$.

Figures 40 through 42 below present the results for, respectively, the displacement u, rotation vector ϕ_i and moment tensor M_{ij} along the ring of nodes located at $r = 234.8$ in. In all cases, the numerically calculated results are highly accurate. Figure 43 shows the results for the shear vector V_i along a ring passing through the centers of the quadrilaterals located at $r = 242.1$ in, and these numerical results, also, are highly accurate.

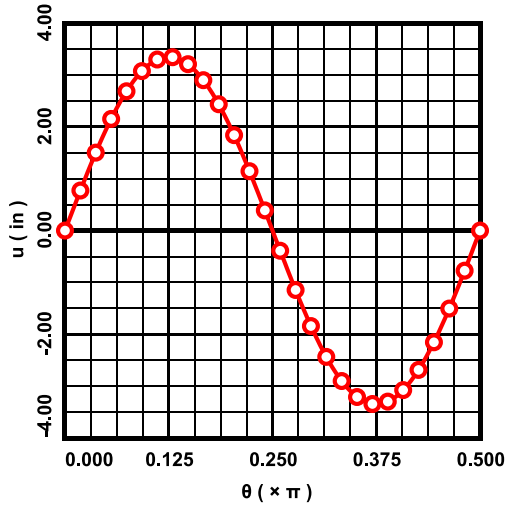

Figure 40. Results for displacement u at $r = 234.8$ in.

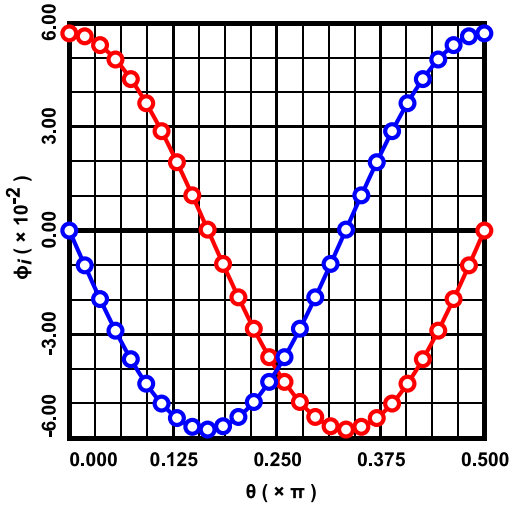

Figure 41. Results for rotation components ϕ_x (red) and ϕ_y (blue) at $r = 234.8$ in.

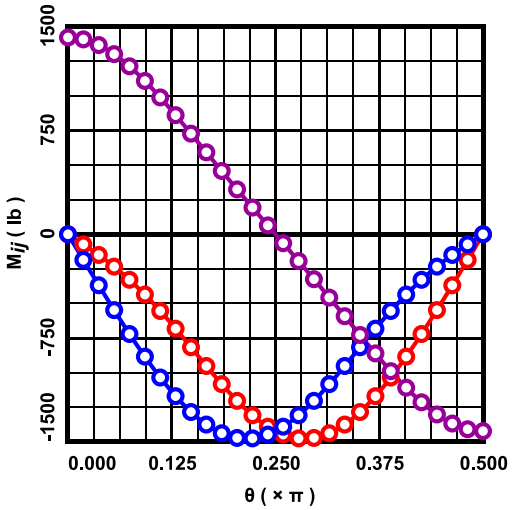

Figure 42. Results for moment components M_{xy} (red), M_{yx} (blue) and M_{xx} (purple) at $r = 234.8$ in.

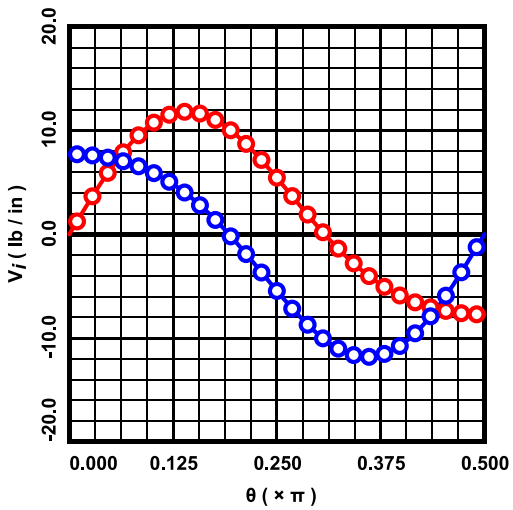

Figure 43. Results for shear components V_x (red) and V_y (blue) at $r = 242.1$ in.

Finally, as for the corner forces at: $(r, \theta) = (b, 0)$, which force is downward; and at $(r, \theta) = (b, \pi/2)$, which force is upward, the numerically calculated magnitudes (are both) 3862.8 lb, and the exact magnitudes are 3935.9 lb, *cf.,* the table at the end of **§4**. The relative error is 1.86%.

10. Closing Remarks

The problem in Cartesian coordinates presented in **§8** is easy to solve numerically. In fact, due to the rectangular elements, the simpler, 12–degree of freedom tensor product cubic element probably would perform just as well.

The problem in polar coordinates presented in **§9**, though, is more difficult to solve. While the numerical values obtained for the nodal values of the displacement u, rotation vector ϕ_i and moment tensor M_{ij} are, for the most part, highly accurate, the numerical values of the shear vector V_i, in some instances, exhibit significant inaccuracy near the boundaries of the domain. Nevertheless, one supposes that using a more refined grid would increase the accuracy of the numerically calculated shear vector components. Perhaps also the procedure used in **§5** to condense out the mid-side nodes is responsible for the inaccurate calculation of the shear components within the triangles (by using the third gradients of the shape functions 5.9). While it may be possible that a 12–degree of freedom tensor product cubic element formulated in polar coordinates would perform well for this problem, this is not an optimal solution, since such an element would be valid only for domains consisting of sectors of annuli.